Flomeko 2000 - IMEKO TC9 Conference
Salvador, Bahia, BRAZIL
4-8 June, 2000

THE EFFECTS OF ASYMMETRIC FLOWS IN THE CORIOLIS MASS FLOWMETER WITH STRAIGHT PARALLEL TUBES: NUMERICAL SIMULATION

P. Kesic and V. Damic***
*University of Zagreb, Faculty of Mechanical Engineering and Naval Architecture, Lucica 4, ZAGREB, CROATIA.
** Polytechnic of Dubrovnik, Cire Carica 4, DUBROVNIK, CROATIA.

Abstract: The effects of flow disturbances on the performance of the Coriolis mass flowmeter(CMF) with two straight parallel tubes were invetigated numerically. Two types of flow disturbances were studied numerically using the bond-graph presentation. The first one represents a local restriction in one of the pipes that causes asymmeric flow in pipes. In the second case of operating conditions, uniformly obliterated tubes were considered. The effect of the obliterated layer thickness with different densities was analysed. It was found that the local restriction at the tube entrance does not effect the sensitivity coefficient, while the flowrate in the tube changes from zero to a rate equal to that in the parallel tube. The obliteration does not effect the sensitivity coefficient either, but changes the first natural mode of tube vibration. If the CMF is used for density measurement, the obliteration may cause significant error.

Keywords: Coriolis mass flowmeter, mass flowmeter, fluid flowrate, bond graphs, flow modelling, flowmeter installation effect.

1. INTRODUCTION

After the Coriolis mass flowmeter (CMF) with a single tube was found to be sensitive to the vibration of the connecting process pipes, a CMF with two parallel vibrating tubes was developed. The tube motion is measured relatively with one in respect to the other. The total flowrate is presumably split into two equal quantities due to the symmetric boundary conditions at the tube inlet and outlet. In real operating conditions there are two types of tube blockage. The first one is a local restriction at the tube ends or in the metering tube. This flow restriction causes the partial or complete blockage of one of the tubes and an asymmetric (unequal) flow in the two tubes. The second type of flow restriction studied here is a uniform build-up in the tubes (obliteration). The obliteration layer causes a flow restriction, even though the flow is split into two equal flowrates.

Since the calibration coefficient (or its inverse, the sensitivity coefficient) is determined under the reference and ideally clean conditions that provide equal flowrates through each tube, it was necessary to analyse the effects of the local restriction and the tube obliteration on the sensitivity coefficient. No experimental data were found on any of the above phenomena, so the problem was studied theoretically. The theoretical analyses of the CMF are not simple and are so far not complete. Sultan and Hemp [1] as well as Rosellier and Durst [2] assumed that the flowrate in the CMF is divided equally, so that the theoretical analyses were reduced to a single tube flowmeter. Recently, Kesic and Damic [3,4] have considered the CMF consisting of two straight parallel tubes as a distributed system and applied the bond graph modelling approach to solve the sensitivity coefficient. Kesic, Damic and Ljustina [5] have also studied the density effect on the sensitivity coefficient.

In this paper the same method was used to study the effects of the two types of flow restriction described above. It is assumed that the flow is uniform in both tubes and no flushing or cavitation occurs in the metering tubes. It is supposed that the eventual build-up has mass and is evenly distributed along the tubes without changing the elastic properties of the tubes. The effects of different

obliteration layer thicknesses and densities were analysed. The meter performance studied here is based on the geometric and material data available for one commercially available CMF.

2. MODELLING AND SIMULATION OF THE CMF

In Fig. 1 the CMF with two straight parallel tubes is shown. The driver is located at the tube midpoint position and the two motion sensors (MS_1 and MS_2) at an equal distance from the walls. At a no-flow condition (Figure 1.b), both motion sensors have the same outputs. In the presence of flow (Figure 1.c), there is a phase shift between the two outputs. This phase shift is directly proportional to the mass flowrate. Instead of the phase shift, the time delay between two signals is measured.

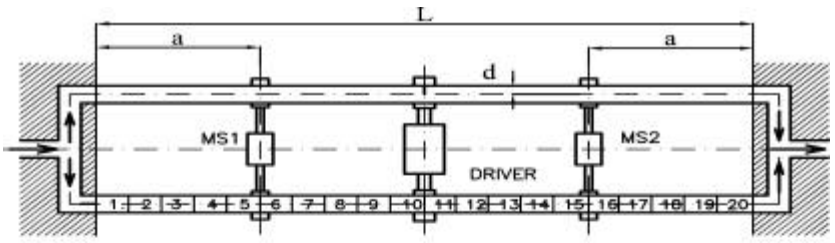

a) Tubes in neutral position.

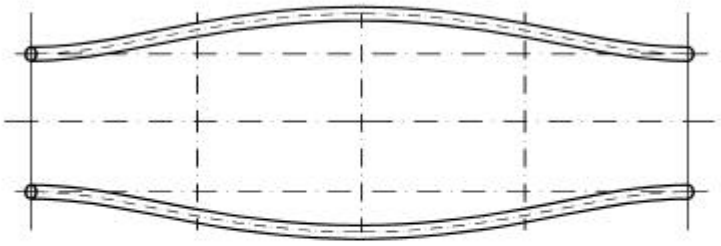

b) Tubes vibrate with no flow.

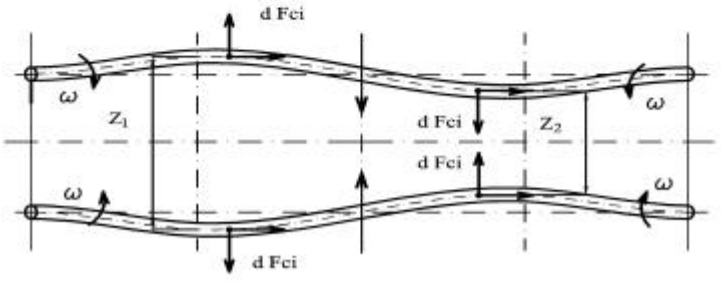

c) Tubes with flow at the instant when driver moves through the neutral position.

Figure 1. Coriolis mass flowmeter with parallel tubes - principle of operation

The equation of motion of the straight tube with fluid flow is given in [2]. However, if the term that includes the fluid velocity dependence is added, it becomes

$$(m_t + m_f)\frac{\partial^2 w}{\partial t^2} + 2m_f U\frac{\partial^2 w}{\partial t \partial x} + m_f \frac{\partial^2 w}{\partial x^2}U^2 + m_f \frac{\partial w}{\partial x}\frac{\partial U}{\partial t} + EI\frac{\partial^4 w}{\partial x^4} = 0 \quad (1)$$

where w is transverse displacement, x is a co-ordinate along the tube axis, m_t and m_f are mass per unit length of tube and of fluid contained in the tube respectively. The uniform fluid velocity in the tube is denoted by U, and E represents the Young modulus of elasticity. The tube cross section moment of inertia is denoted by I, and L_t is the tube length. Both tube ends are clamped so that the boundary conditions are

$$w(0) = w(L_t) = 0 \quad (2)$$

$$\left(\frac{\partial w}{\partial x}\right)_{x=0} = \left(\frac{\partial w}{\partial x}\right)_{x=L_t} = 0 \quad (3)$$

The sensing pipe of length L_t is split into finite tube elements of equal lengths L. In Fig. 2.a the finite element is shown. The boundary conditions for each element are given by

$$F1 = EI\frac{\partial^3 w}{\partial x^3}(0), M1 = -EI\frac{\partial^2 w}{\partial x^2}(0)$$
$$F2 = EI\frac{\partial^3 w}{\partial x^3}(L), M2 = -EI\frac{\partial^2 w}{\partial x^2}(L) \quad (4)$$

However, for the first and the last final element the conditions given by equations (2) and (3) are valid at the walls.

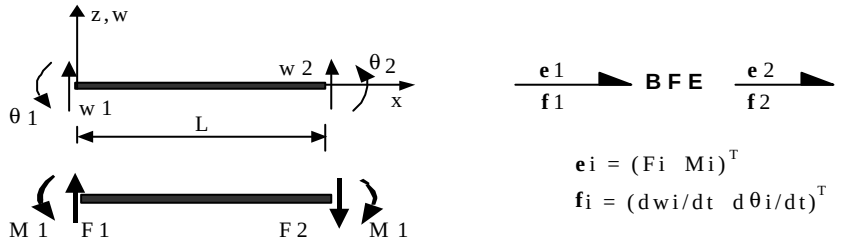

a) b)

Figure 2. Finite element and the node variables

The spacional discretisation was applied using the Galerkin finite element method and cubic shape functions (Smith and Griffiths [6]). The resulting equations in matrix notation are

$$\boldsymbol{M}\frac{d^2\boldsymbol{w}}{dt^2} + 2\boldsymbol{R}U\frac{d\boldsymbol{w}}{dt} + (\boldsymbol{K} + \boldsymbol{R}\frac{dU}{dt} + \boldsymbol{C}U^2)\boldsymbol{w} = \boldsymbol{F} \quad (5)$$

where $\boldsymbol{w}$ is the vector of section displacement and of angle rotation at two nodes of the element. Matrices $\boldsymbol{M}$ and $\boldsymbol{K}$ are well known consistent mass and stiffness matrices respectively. The $\boldsymbol{R}$ and $\boldsymbol{C}$ matrices take into account Coriolis, and centripetal acceleration effects and are given by

$$\boldsymbol{R} = \frac{m_f}{2}\begin{bmatrix} -1 & L/5 & 1 & -L/5 \\ -L/5 & 0 & L/5 & -L^2/30 \\ -1 & -L/5 & 1 & L/5 \\ L/5 & L^2/30 & -L/5 & 0 \end{bmatrix} \quad (6)$$

$$\boldsymbol{C} = \frac{m_f}{L}\begin{bmatrix} -6/5 & -11L/10 & 6/5 & -L/10 \\ -L/10 & -2L^2/15 & L/10 & L^2/30 \\ 6/5 & L/10 & -6/5 & 11L/10 \\ -L/10 & L^2/30 & L/10 & -2L^2/15 \end{bmatrix} \tag{7}$$

where L is tube element length. ***F*** is the vector of the prescribed forces and moments at the nodes

$$\boldsymbol{F} = (F1\ M1\ -F2\ -M2)^T \tag{8}$$

It should be noted that matrix ***R*** is not strictly antisymmetric. The elements on the main diagonal of the matrix, corresponding to the transverse displacement at the connected nodes, are 1 and -1. Thus, after assembly, they cancel out so the overall matrix is antisymmetric. A similar conclusion can be drawn regarding the symmetry of the ***C*** matrix.

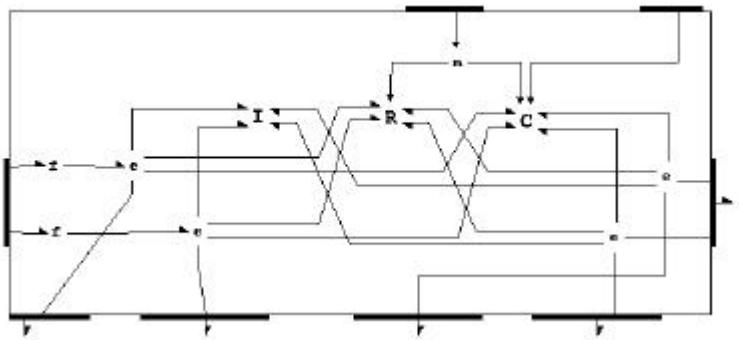

Figure 3. Bond graph model of the tube element

The equations (4) to (7) can be represented in the form of a bond graph as given in Figure 3. The graph is used as a functional description of the Bond graph finite element BFE in Figure 2.b. The complete process is carried out with the help of Bond graph modelling and the simulation program BondSim described in Damic and Montgomery [7]. The program supports the developing of a model in a hierarchical fashion.

The model clearly shows the basic physical interaction in the tube element. The model consists of three interconnected four-port components, I, C and R. Component I represents the accumulation of the kinetic energy of the tube and the fluid contained in the tube, C represents the accumulation of potential energy and R describes the Coriolis coupling. Nodes e and f describe the balancing of efforts (forces and torques) and of flows (linear and angular velocities) at the tube element nodes respectively. There is no real dissipation of energy in the system because of the coupling forms as described by the equation (6). The constitutive relations corresponding to the terms in equation (5) and to matrices ***M***, ***R***, ***K*** and ***C*** are described in a symbolic form that closely follows the original formulation. Connecting the ports of the components creates a bond graph super-element. By connecting several super-elements it is possible to develop a higher level super-element and so on. In this way a model of the flow-meter tube consisting of a large number of finite elements can be developed in a straightforward manner. In this paper, tube models with 4, 20 and 100 BFE are studied.

The model of the complete sensor is shown in Figure 4. The model consists of the measuring tubes, driver and two sensors. Currently, the driver is not modelled as a real electromechanical device but simply as a half sinus pulse force generator. The duration of the pulse is taken to be equal to a period of the first mode vibrations in the case of no flow. Information on element node displacements corresponding to the position of the sensors are picked up and fed back to an x-t display window. The sum a_{sum} and the difference a_{diff} of signals are also formed and displayed. The metering tubes are clamped to the walls and fluid flows are given as the signal inputs to the tubes. The corresponding outputs are fed to the display.

The study of flowmeter behaviour is conducted by simulation. The program automatically generates a mathematical model of the measuring system in the form of a large set of algebraic and differential

equations (DAE) in symbolic form. The equations are solved during the simulation run by a suitable DAE solver.

In commercial Coriolis flowmeters there are quite elaborate techniques for the detection of signal delay between the zero crossings of two signals, the frequency of vibrations, etc. In this study, this information is obtained from the frequency spectrum of the sum of sensor signals and their difference. The spectrums are evaluated by a Fast Fourer Transform software module. The time delay was calculated according to the formula [7]

$$\Delta t = \frac{a_{dif}}{\pi a_{sum} f} \tag{6}$$

where a_{sum} and a_{diff} are amplitudes of the sum and the diference of signals from the motion sensors at the frequency of oscilation f (first mode) as determined numerically.

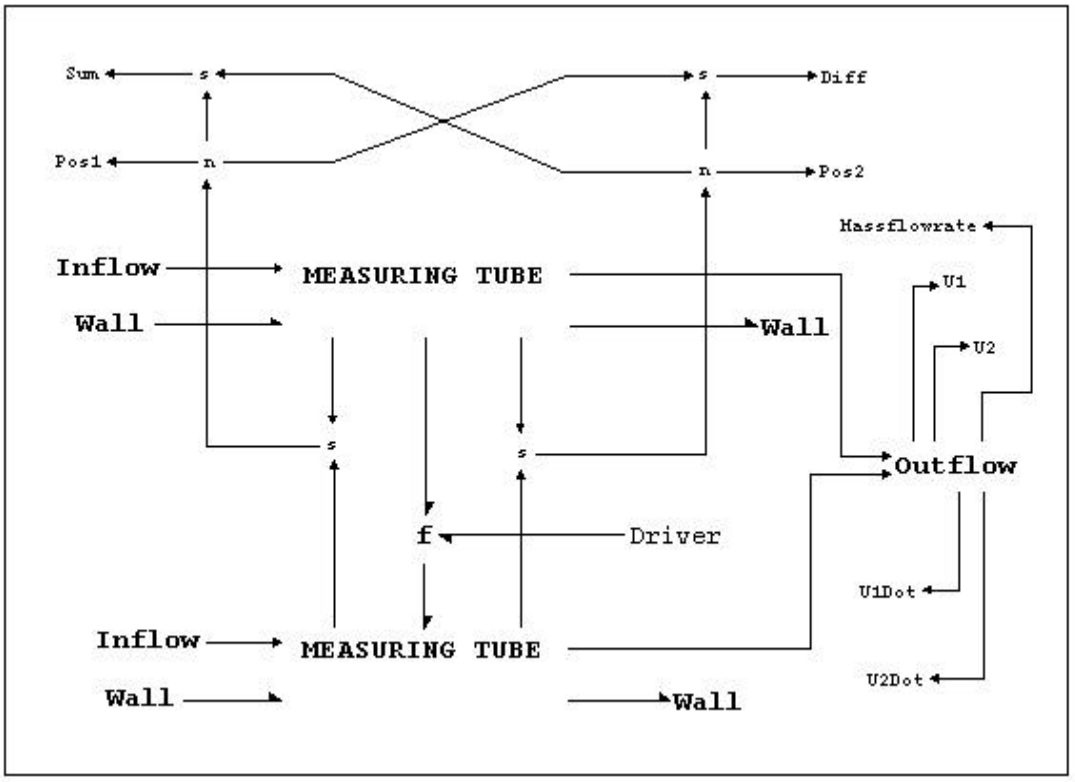

Figure 4. *Model of Coriolis mass flowmeter with two straight parallel tubes*

3. SIMULATION RESULTS FOR UNDISTURBED FLOWMETER

The CMF performances were calculated using the basic tube parameters from one well-known meter manufacturer. The geometric tube parameters are: outside diameter D = 39.5 mm, inside diameter d = 37.5 mm and length L_t = 1343 mm. The physical parameters are: material density ρ_t = 8000 kg/m^3, Young model of elasticity E = 195 GPa. The two different motion sensor locations are considered. In the first case, the motion sensors are located at a distance of 1/4 L_t from the clamping points and in the second case at a distance of 3/20 L_t. The fluid velocity was varied from 0 to 15 m/s.

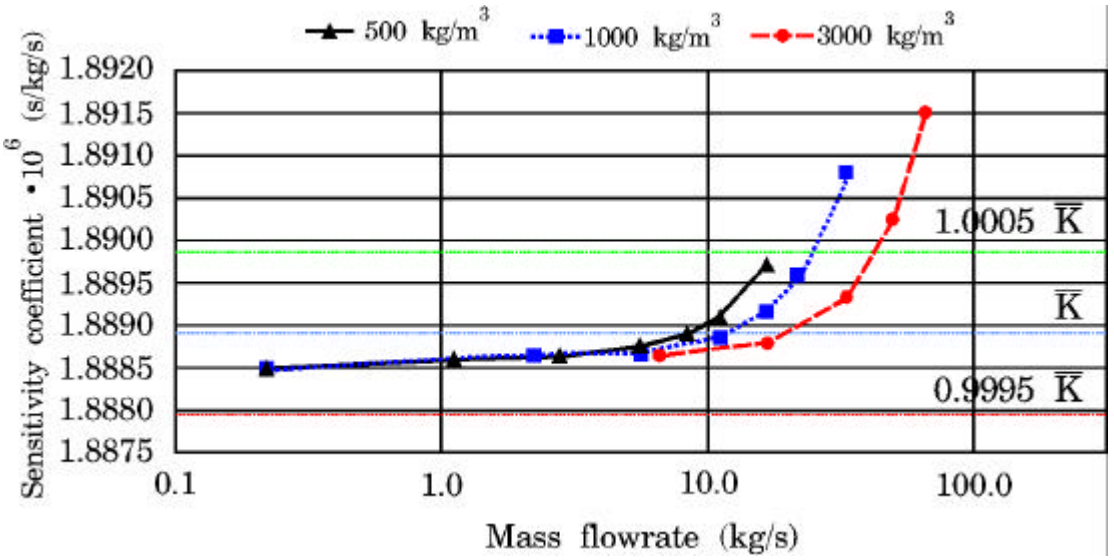

Figure 5. Sensitivity coefficient as a function of mass flowrate

The sensitivity coefficient as a function of mass flowrate for the three different densities is presented in Figure 5. The average value of the sensitivity coefficient K=1.8889 10^{-6} s/(kg/s) was determined based on the sensitivity coefficient values for fluid density of 1000 kg/m^3 in the velocity range from 0.1 to 10 m/s. If the maximum mass flowrate (Q_m= 22.09 kg/s) is determined at the fluid velocity of 10 m/s and a density of 1000 kg/m^3, the theoretical linearity of this flowmeter is better than ±0.05%. Higher velocities are not practical due to the large pressure drop. For fluid densities larger than 1000 kg/m^3, the linearity range can be extended toward higher mass flowrates, but again at the expense of higher pressure loss. For a fluid with a density of 500 kg/m^3 , the linearity limit of ±0.05% is reached at about 17 m/s but at a smaller mass flowrate than the maximum determined with a fluid density of 1000 kg/m^3 (density of water at the reference condition).

The calculated natural frequency (the first mode) f_0 = 90.69 Hz and the sensitivity K=1.8889 10^{-6} s/(kg/s) differ from the manufacturer's averaged data of f_m = 118.7 Hz and K_m=1.205 10^{-6} s/(kg/s). This difference is probably caused by boundary conditions which are not uniquely defined. In the real design there are braces located between the clamping and the sensing points that increase the tube stiffness. Following Sultan and Hemp [1], the equivalent length is defined for which the calculated and the measured frequencies are equal. The equivalent length of L_t =1175mm provides the first mode natural frequency f_0 = 118,6 Hz and the sensitivity K=1,261 µs/(kg/s) that are close to the averaged measured values. In addition, if the motion sensors are placed at a distance of L_t/3 from the clamping ends, the numerical values for the tube frequency and the sensitivity factor become again very close to the manufacturer's values.

4. SIMULATION RESUILTS FOR DISTURBED FLOWMETER

The two types of flow disturbance studied here are shown in Figure 6. The effects of the flow asymmetry due to the first type of restriction are shown in Table1. The fluid velocity in the first tube was varied from 5 m/s to 0 m/s while at the same time it was increased from 5 m/s to 10 m/s in the second tube. A comparison of the data in the first four rows shows that there is no change in the sensitivity coefficient, even though the flowrate in the second tube is four times higher than in the first one. Even in the case where the first tube is completely blocked (V1=0), the sensitivity coefficient is only 0.2% smaller than for the symmetric case. The last two lines show the quality of the numerical calculation. Here the intensity of the flowrate is exchanged between the tubes. There is no significant difference in the sensitivity coefficient. The mass flow rate remained 11.04 kg/s in all cases. Similar results were obtained for the mass flowrate of 2.209 kg/s where the fluid velocity in the first tube varied from 0 to 2 m/s and in the second tube from 2 to 4 m/s. The results of the simulation are shown in Figure 7. In both cases the sensitivity coefficient remains well within ±0.05% tolerance.

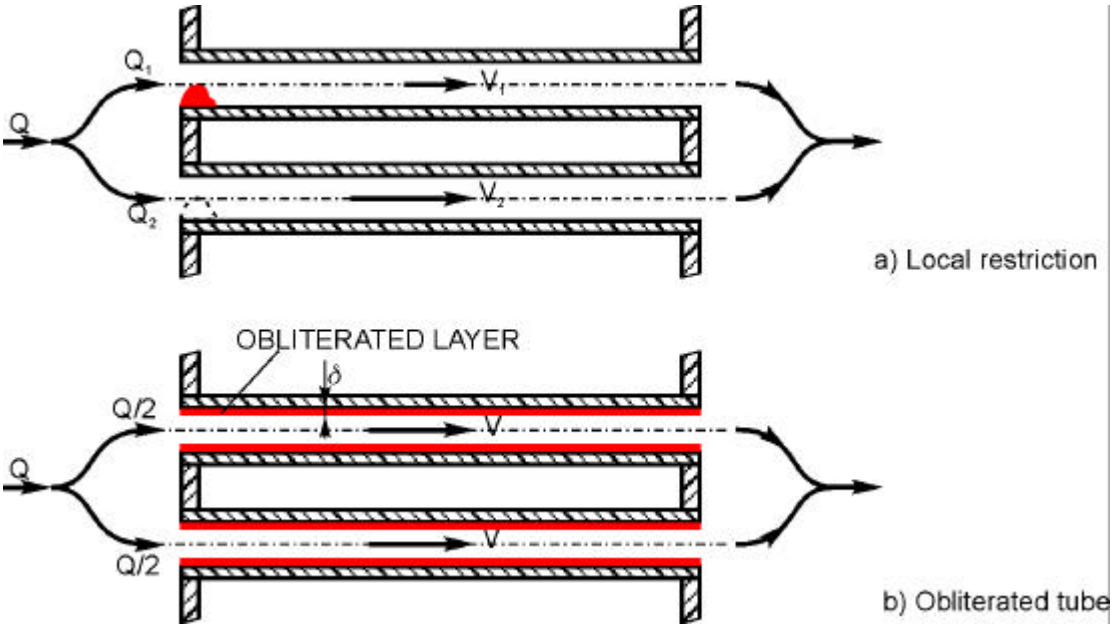

Figure 6. Two types of flow restrictions

Table1 Model with two parallel tubes, ρ_f = 1000 kg/m3, 20 FE, motion sensors at positions between 5th and 6th and between 15th and 16th elements. Input fluid velocities are V1 and V2, respectively

V1 (m/s)	V2 (m/s)	Qm (kg/s)	Asum (m)	Adiff (m)	f (Hz)	Delay (s)	K (s/(kg/s)
5	5	11.044662	3.642474E-03	2.164769E-05	90.6803	2.086183E-05	1.88886E-06
4.5	5.5	11.044662	3.642754E-03	2.164958E-05	90.68013	2.086208E-05	1.88888E-06
4	6	11.044662	3.642809E-03	2.165044E-05	90.67964	2.086271E-05	1.88894E-06
2	8	11.044662	3.643386E-03	2.165967E-05	90.67441	2.086950E-05	1.88956E-06
0	10	11.044662	3.644538E-03	2.167880E-05	90.66395	2.088374E-05	1.89084E-06
10	0	11.044662	3.644542E-03	2.167883E-05	90.66395	2.088375E-05	1.89085E-06

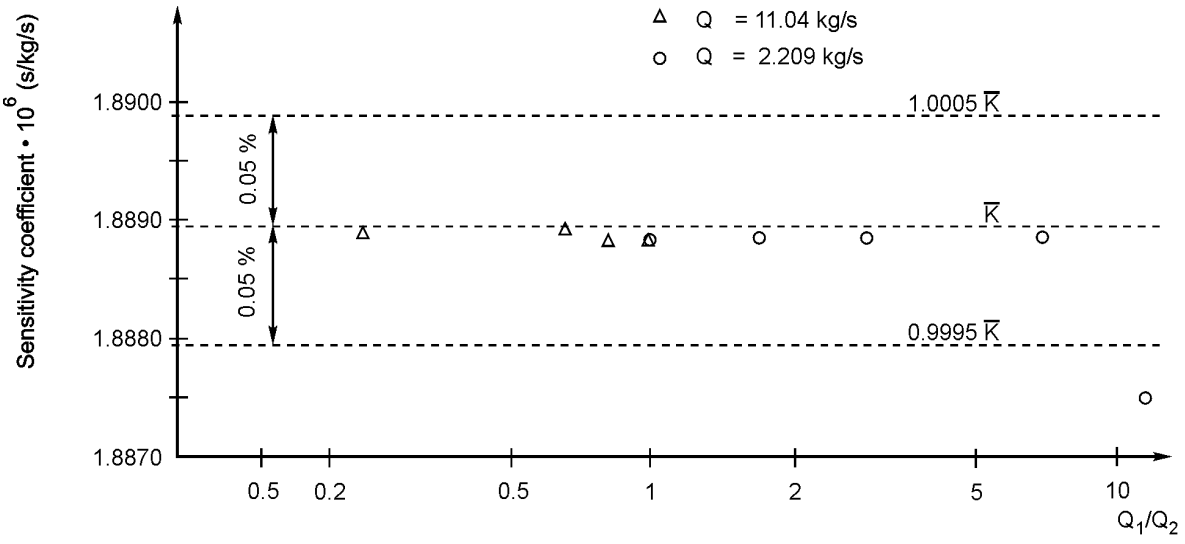

Figure 7. Effect of the local restriction on the sensitivity coefficient

The effects of obliteration were studied for the two thicknesses (1 mm and 5 mm) and the two densities (1000 kg/m^3 1200 kg/m^3). The simulation results for the obliteration layer thickness of 5 mm and a density that is 20 % higher than the fluid density are shown in Table 2.

Table 2 Obliterated tube: ρ_f = 1000 kg/m3, 20 FE, obliteration thickness 5.0 mm and relative density (with respect to fluid density) equal to 1.2

V [m/s]	Q_m [kg/s]	A_{sum} [m]	A_{diff} [m]	f [Hz]	Delay [s]	K [s/(kg/s]
1	1.187914722	3.780740E-03	2.359610E-06	88.5437	2.243654E-06	1.888733E-06
2.5	2.969786805	3.781330E-03	5.899560E-06	88.5422	5.608863E-06	1.888642E-06
5	5.939573611	3.782110E-03	1.180150E-05	88.5365	1.121840E-05	1.888755E-06
7.5	8.909360416	3.783020E-03	1.770600E-05	88.5271	1.682890E-05	1.888901E-06
10	11.87914722	3.785130E-03	2.362060E-05	88.5139	2.244134E-05	1.889137E-06

The deposit reduces the inner diameter from 37.5mm to 27.5mm. In all cases the deposit does not change the sensitivity coefficient. However, a denser deposit changes the natural frequency by 2.4%. If the natural frequency is used for fluid density measurement, then the natural frequency change of 2.4% leads to a 9.0% error in the density results [5]. The obliteration effects for all thicknesses and densities studied here are shown in Figure 8. No significant effect was found on the sensitivity coefficient within the velocity range studied.

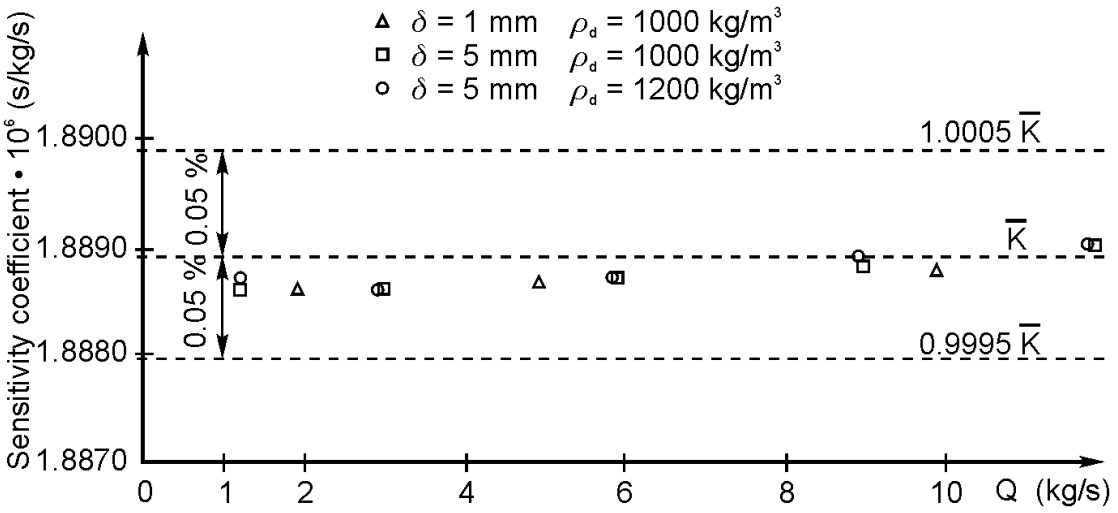

Figure 8. Effect of obliteration on the sensitivity coefficient

5. CONCLUSIONS

The analysis in this paper showed that:

1. The theoretical linearity of the CMF meter was very low (0.05%) over a wide flowrate range. The maximum mass flowrate with the defined linearity depends on density. The mass flowrate increases with an increase in density.
2. The flow disturbance that reduces flow in one of the tubes did not effect the sensitivity coefficient.
3. Tube obliteration with a deposit of the same density as the fluid density or even 20% higher did not change the sensitivity coefficient. However, denser deposits changed the natural frequency of the tube. If the CMF is used for density measurements in the presence of obliteration, significant errors may occur.

4. BondSim successfully solved the problem of fluid motion in the CMF. The flowmeter model can be easily modified to include more realistic models of driver, sensors, signal processing, operating conditions, installation conditions etc.

LITERATURE

[1] G. Sultan and J.Hemp," Modelling of the Coriolis Mass Flowmeter", Journal of Sound and Vibration, 1989, 32(3), pp. 473-489.
[2] H. Rasillier and F. Durst," The Coriolis-Effect in Mass Flow Metering", Archive of Applied Mechnaics, 61(1991), 192-214.
[3] P. Kesic and V. Damic, " The Coriolis Mass Flowmeter and the Fluid Angular Rate Gyro: A Unified Approach and Simulation", Flomeko98, Lund, Sweden, 1998, pp 249-254.
[4] P. Kesic, and V. Damic, "The Coriolis Mass Flowmeter with Elastic Parallel Tubes: Mathematical Model and Numerical Solution", Metrologie 99, 9-th International Metrology Congress, Bordex, France, pp. 472-475, 1999.
[5] P. Kesic, V. Damic and A.M. Ljustina," Modelling of the Mass Flowmeter with Straight Parallel Tubes", Nafta, March 2000(51), No.3, Zagreb, pp. 91-98.
[6] I.M Smith and D.V. Griffiths, Programming the finite element method, 3rd ed., John Wiley & Sons, 1998, pp. 21-27.
[7] V. Damic and J. Montgomery, "Bond Graph Based Automated Modelling Approach to Functional Design of Engineering Systems", Proceedings of Mechanics in Design '98 International Conference, The Nottingham Trent University, Nottingham, UK, 1998, pp. 377-386.

Author(s): Prof. Dr. P. Kesic, University of Zagreb, Faculty of Mechanical Engineering and Naval Architecture, Lucica 4, ZAGREB, CROATIA, Fax: +385 1 615 6 940; E-mail: petar.kesic@fsb.hr; Prof. Dr. V. Damic, Polytechnic of Dubrovnik, Cire Carica 4, DUBROVNIK, CROATIA, Fax:+ 385 02 435 590, E-mail: vjeko@vdu.hr.